Available online at www.sciencedirect.com
ScienceDirect
Earth and Planetary Science Letters 261 (2007) 578 – 589
EPSL
www.elsevier.com/locate/epsl

Giant landslides, topography, and erosion

Oliver Korup [a,*], John J. Clague [b], Reginald L. Hermanns [c], Kenneth Hewitt [d], Alexander L. Strom [e], Johannes T. Weidinger [f]

[a] Swiss Federal Research Institutes WSL/SLF, CH-7260 Davos, Switzerland
[b] Department of Earth Sciences, Simon Fraser University, Vancouver B.C., Canada
[c] Geological Survey of Canada, Vancouver B.C., Canada
[d] Cold Regions Research Centre, Wilfrid Laurier University, Waterloo, Canada
[e] Institute of Geospheres Dynamics, Russian Academy of Sciences, Moscow, Russia
[f] Department of Geological Sciences, University of Salzburg, Austria

Received 26 February 2007; received in revised form 16 July 2007; accepted 16 July 2007
Available online 24 July 2007
Editor: C.P. Jaupart

Abstract

Distributions of slope angles in tectonically active mountain belts point to the development of threshold conditions, where hillslopes attain a critical inclination or height at which they fail readily because of limitations in material strength. It has been proposed that hillslopes adjust to rapid uplift and bedrock incision through an increase in the rate of relief-limiting landsliding rather than gradual slope steepening. Here we test this concept by investigating the relationship between mean local relief $\bar{H}$, which we take to be a proxy of long-term erosion rates E, and the occurrence of over 300 of the largest ($V > 10^8$ m^3) terrestrial landslides on Earth. We find that nearly two-thirds of these giant landslides have occurred in the steepest 5% of the Earth's land surface, where relief is close to its proposed upper strength limit. They are primarily located in deeply incised valleys, along fault-bounded fringes of active mountain belts, and in volcanic arcs.

This distribution coincides with areas of high long-term erosion rates (~4 mm yr^{-1}), confirming that giant landslides contribute to rapid denudation of mountains. Most of the eroded volume is concentrated in the smallest, but steepest parts of mountain belts and volcanic arcs. First-order estimates of minimum erosion rates accomplished by the largest landslides are ≥ 0.01 mm yr^{-1}; these rates are between 1% and 10% of the Late Pleistocene to Holocene mean erosion rates in a given area. Importantly, the landslide erosion rates show a nonlinear increase with mean local relief, suggesting that the contribution of giant landslides in total and per event increases significantly with increasing overall erosion rates. However, giant landslides also occur in areas of lower-than-average relief ($\bar{H} \sim 300$–700 m), irrespective of whether threshold hillslopes have developed or not. Factors contributing to these failures include soft rocks, extensive low-angle discontinuities, high rates of fluvial bedrock incision, and tectonically driven deformation and slope loading.

Keywords: landslide; mean local relief; mountain topography; erosion

1. Introduction

Catastrophic landslides are localised, but highly efficient agents of erosion in mountainous terrain, moving

* Corresponding author. Tel.: +41 81 417 0250; fax: +41 81 417 0110.
E-mail address: korup@slf.ch (O. Korup).

0012-821X/$ - see front matter © 2007 Elsevier B.V. All rights reserved.
doi:10.1016/j.epsl.2007.07.025

large masses of material over kilometre-scale distances in geologically instantaneous time ($\sim 10^2$ s) (Eisbacher and Clague, 1984). Because they are frequently triggered by earthquakes and high-intensity precipitation events, their study provides insight to tectonic and climatic forcing of hillslope adjustment to topographic relief produced by glacial erosion and fluvial bedrock incision.

It has been proposed that hillslopes in active mountain belts adjust to high rates of rock uplift and erosion by increases in the rate of landsliding rather than by progressive slope steepening (Montgomery and Brandon, 2002). This hypothesis implies that hillslopes attain a threshold angle characteristic of limit equilibrium conditions of slope failure that is insensitive to changes in uplift, climate, or lithology (Burbank et al., 1996; Montgomery, 2001). Hillcrests and divides are worn down at a rate that effectively maintains local hillslope relief.

Montgomery and Brandon (2002) argued that topographic relief cannot grow indefinitely, proposing a hyperbolic relationship between the long-term erosion rate E and orogen-scale mean local relief $\bar{H}$ for tectonically active mountain belts throughout the world:

$$E = E_0 + \frac{K\bar{H}}{[1-(\bar{H}/H_c)^2]}, \tag{1}$$

where E_0 is the erosion rate due to chemical weathering, K is a rate constant, and H_c is the limiting relief. This relationship implies that, for regions that have a mean local relief close to H_c, small increases in mean local relief require substantial increases in erosion rates. Montgomery and Brandon (2002) proposed that hillslope and relief adjustment to high rates of erosion is achieved through increases in the rate of landsliding rather than slope steepening.

From an engineering geological perspective, key controls on hillslope stability include material strength set by cohesion and internal friction, slope and discontinuity geometry, and transient loading imposed by water content and seismic ground acceleration. For simple solutions, limit equilibrium conditions of landsliding can be expressed as a maximum stable hillslope height, supporting the notion of landslide-limited relief (Schmidt and Montgomery, 1995). It has also been proposed that erosional unloading by valley incision or debuttressing during deglaciation alters topography-induced stress fields, focusing tensile stresses near valley floors and thus further disposing slopes of sufficient relief to catastrophic failure (Augustinus, 1995).

In numerical studies of landscape evolution, landslide triggering can be modelled in terms of attainment of a critical hillslope height or threshold hillslope angle at which slope failure will occur (Densmore et al., 1998). By implication, these thresholds of relief or slope angle cannot be exceeded (Eq. (1)), because they are maintained and limited by landsliding. Threshold hillslopes have been reported from the northwestern Himalaya (Burbank et al., 1996), the Olympic Mountains (Montgomery, 2001), the fringes of the Tibetan Plateau (Whipple et al., 1999), and the New Zealand Southern Alps (Korup, 2006a, b). With few exceptions (Montgomery, 2001), however, there have been no attempts to further validate a causal link between threshold hillslopes and the rates and characteristics of landslides in these or other mountain belts.

Here, we provide one of the first regional-scale tests of the concept of failure-controlled relief limitation at the upper size limit of landsliding. We compiled data on over 300 of the largest catastrophic terrestrial landslides on Earth. We examine these giant landslides with respect to mean local relief and long-term, orogen-scale erosion rates in Earth's major mountain belts. The frequency of landslides is inversely and nonlinearly related to landslide size (Malamud et al., 2004), but the validity of this and other empirical statistical models is limited to inventories containing only a fraction of the landslide size spectrum, i.e. mainly small events. We use the apparent erosion rate of giant landslides as a proxy of their overall rate of landsliding. This approximation seems reasonable, as we are interested in the response of giant landslides to changes in topographic relief, rather than the general relationship between magnitude and frequency of landsliding itself.

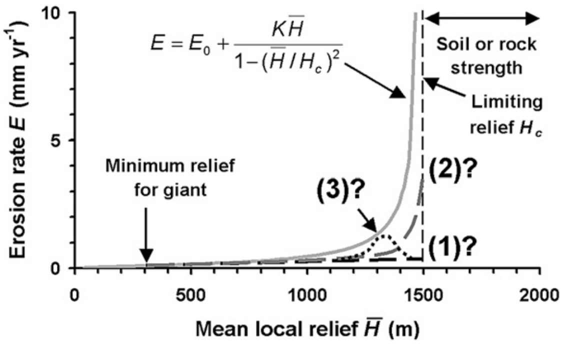

Fig. 1. Nonlinear relationship between long-term erosion rate E and mean local relief $\bar{H}$ proposed by Montgomery and Brandon (2002) (grey curve; Eq. (1)). The contribution to erosion rates of giant landslides (exaggerated here for clarity) may have a variety of hypothetical forms: (1) linear; (2) hyperbolic; or (3) complex with an intermediate maximum. See text for explanation.

We hypothesize that if the nonlinear relation between erosion rates and mean local relief is indeed governed by the rate of landsliding (Montgomery and Brandon, 2002), the contribution of large events should also increase with growing topographic relief (Fig. 1). In the alternative cases of invariant or declining rates of erosion by giant landslides, we would expect a higher contribution from smaller landslides in order to account for the necessary increases in erosion rates. Our study addresses several key questions of how topography and landslides dynamically interact: What are the relationships between topographic relief and the largest landslides on Earth? Is the spatial distribution of these giant slope failures fully explained by hillslope relief? How do these landslides contribute to relief adjustment and erosion? We first present results from a regional quantitative analysis. In the discussion, we refine these findings based on our field observations on giant landslides in various mountain belts.

2. Landslide inventory

We compiled an inventory of catastrophic terrestrial landslides larger than an arbitrary threshold of 10^8 m^3, allowing for a 10% error margin because of uncertainties in estimating landslide volumes (Fig. 2A). Our dataset includes over 300 landslides and substantially augments previous worldwide and regional inventories (Siebert et al., 1987; Shaller, 1991; Beetham et al., 2002; Capra et al., 2002; Wen et al., 2004; Bookhagen et al., 2005; Ponomareva et al., 2006). It also includes data from our own studies (Eisbacher and Clague, 1984; Hewitt et al., 1998; Hewitt, 2001; Hermanns and Strecker, 1999; Korup, 2006a, b; Strom and Korup,

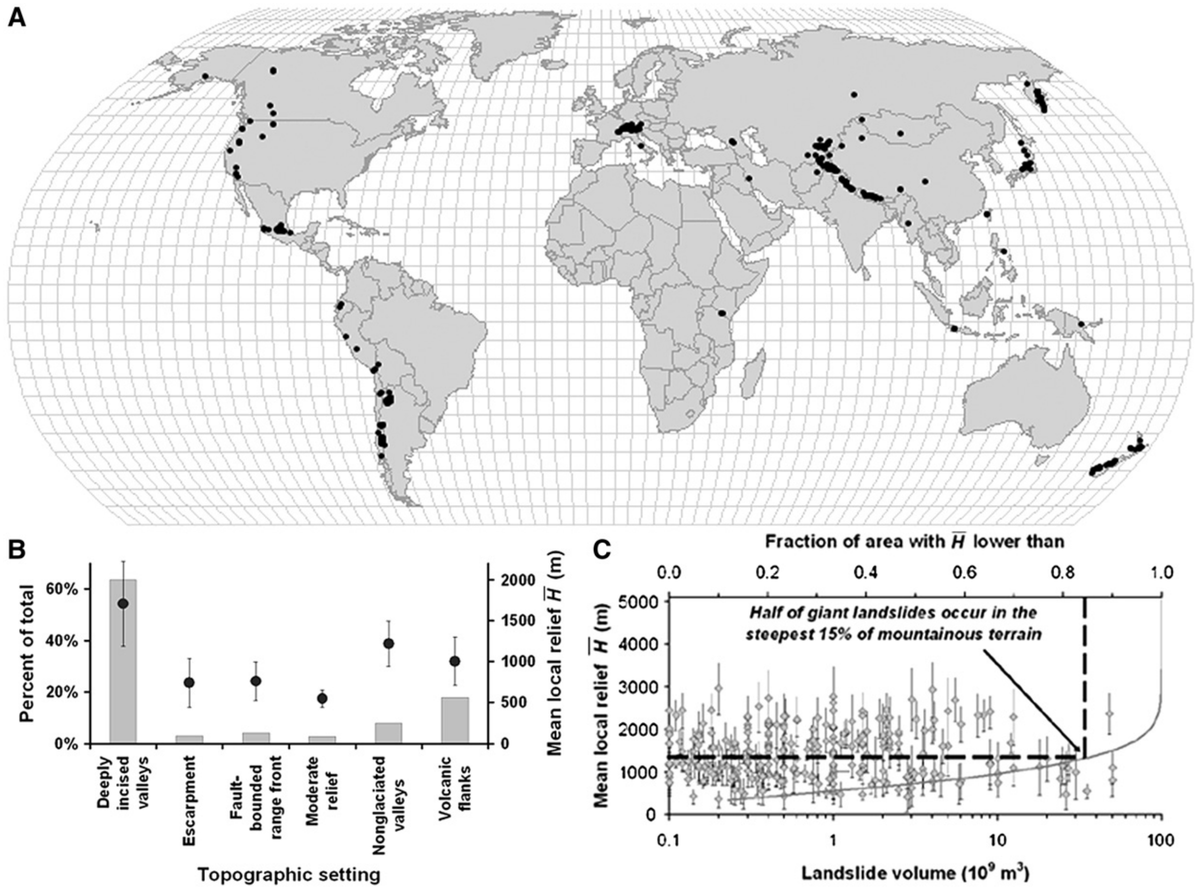

Fig. 2. A. Worldwide distribution of giant landslides ($V > 10^8$ m^3) used in this study. B. Topographic setting of giant landslides. Grey bars are relative frequency and black dots are mean local relief $\overline{H}$; vertical bars are $\pm 1\sigma$. Local relief H was computed following Montgomery and Brandon (2002) and averaged within a circle of 15-km radius around each landslide site to obtain $\overline{H}$. C. Relationship between $\overline{H}$ and landslide volume (grey diamonds with 1σ bars). Grey curve is sum of cumulative distributions of H in all mountainous regions studied.

2006; Weidinger, 2006). We augmented the dataset by measuring landslide geometries on satellite images and digital terrain models. We did not include submarine landslides or those that descended from subaerial volcanic edifices and entered the sea, although we collected data on terrestrial volcanic debris avalanches. We acknowledge, however, that the largest submarine landslides are at least two orders of magnitude larger than their terrestrial counterparts (Collot et al., 2001; Vanneste et al., 2006). Our analysis is limited to catastrophic, i.e. rapid, landslides and excludes slow failures of a more chronic nature, such as deep-seated gravitational creep or rock flow.

Testing of our hypothesis (Fig. 1) requires that we focus our analysis to the variables specified in Eq. (1). Hence we used the method of Montgomery and Brandon (2002) to compute local relief H. Specifically, we subtracted minimum from maximum elevation within a moving window with radius $r=5$ km for selected mountain belts and volcanic arcs throughout the world. In order to quantify H in a way that smoothes local modifying effects of giant landslides, we computed the average of H, that is the mean local relief $\bar{H}$, for the mountain belts of interest as well as within a 15-km radius around each landslide. Computations were done using SRTM30 global digital elevation data at a nominal resolution of ~860 m. We limited our analysis to terrain with $H>300$ m, which we find adequately captures the extent of major mountain belts and yields orogen-scale values of $\bar{H}$ closely comparable to those of Montgomery and Brandon (2002). We are aware that local slope angle β is a more appropriate parameter than H for investigating first-order and physically-based controls on large-scale slope instability. However, the coarse resolution of the SRTM30 data substantially underestimates values of β, whereas digital elevation models of higher resolution suffer from lack of global coverage, data gaps in steep mountainous terrain, and the modifying effects of giant landslides themselves. In many cases, we found it intractable to reliably reconstruct pre-failure hillslope morphology, let alone slope angles. This problem is partly compensated by the reasonable correlation between H and β demonstrated for the chosen value of $r=5$ km (Montgomery and Brandon, 2002).

3. Giant landslides and topography

3.1. Giant landslides near the limiting relief

About 40% of the giant landslides investigated are late Quaternary in age. Some occurred during the Late Pleistocene, but most are Holocene in age, and at least 26 giant landslides have been recorded in the 20th century. They are typically kilometre-scale events, affecting areas between 10^0 and 10^3 km^2 (Table 1). Nearly two-thirds of the landslides are highly mobile rock avalanches (*sturzstroms*) or volcanic debris avalanches; very few have involved failure of material other than bedrock.

Most giant landslides were identified in deeply incised and formerly glaciated valleys, where $\bar{H}$ is highest (Fig. 2B). Other settings include flanks of volcanoes, escarpments, fault-bounded mountain fronts (Hermanns and Strecker, 1999), and areas adjacent to active major faults (Strom and Korup, 2006; Weidinger, 2006). Catastrophic slope failures in these latter topographic settings tend to have the highest volumes on average. We note that giant landslides occur in all lithologies and climatic settings, but we suspect that their distribution is biased by different degrees of mapping and field investigation.

Nearly 75% of giant landslides have occurred in terrain with mean local relief $\bar{H}>1000$ m, which makes up <5% of Earth's land surface (Montgomery and Brandon, 2002). The terrain includes all major active mountain belts — the European Alps, Caucasus, Himalayas, Pamir, Tien Shan, American Cordilleras, Papua New Guinea, and Southern Alps of New Zealand (Fig. 2A). About 25% of the landslides are debris avalanches in volcanic arcs, such as Kamchatka, Japan,

Table 1
Descriptive statistics of worldwide inventory of over 300 giant ($V>10^8$ m^3), catastrophic landslides

Parameter	n	Min.	Max.	Mean (±1σ)	Median	5% quantile	95% quantile
Volume (10^9 m^3)	343	0.1	81	3.08±8.04	0.57	0.1	14.8
Age (ka)	133	0	350	15.8±50.1	3.3	0.02	43.4
Maximum height (km)	232	0.3	4.5	1.6±0.9	1.5	0.5	3.4
Runout (km)	249	0.8	120	12.1±16.0	6.8	2.1	41.8
Mean deposit thickness (m)	147	5	1000	135±142	97	14	350
Area (km^2)	236	1	2200	83.8±248.1	10	1.7	455
Mean local relief (km)	262	0.37	2.96	1.44±0.58	1.35	0.57	2.43

Central America, and the Andes. More than 50% have occurred in the steepest 15% of these mountain belts, with an average $\bar{H}=1435$ m (Fig. 2C; Table 1). This value is close to the orogen-scale "limiting relief" of Montgomery and Brandon (2002), i.e. $H_c=1500$ m, which separates regions with the highest erosion rates from those where rock-mass strength is sufficient to maintain such high relief (Fig. 1).

At the scale of individual mountain belts, many giant landslides also tend to occur in the steepest part of the landscape. In the Himalayas, for example, most giant landslides have taken place in regions where $\bar{H}$ exceeds the regional mean by one standard deviation (Fig. 3). This condition is met by ~10% of the total terrain with $\bar{H}>300$ m. More than half of giant landslides have occurred in the steepest 6% of the mountain belt, characterized by $\bar{H}\geq 2$ km (Fig. 3). Areas with such high relief include most of the High Himalayas (Weidinger, 2006), the area around Nanga Parbat in the Karakoram (Hewitt et al., 1998), and deeply incised valleys along the

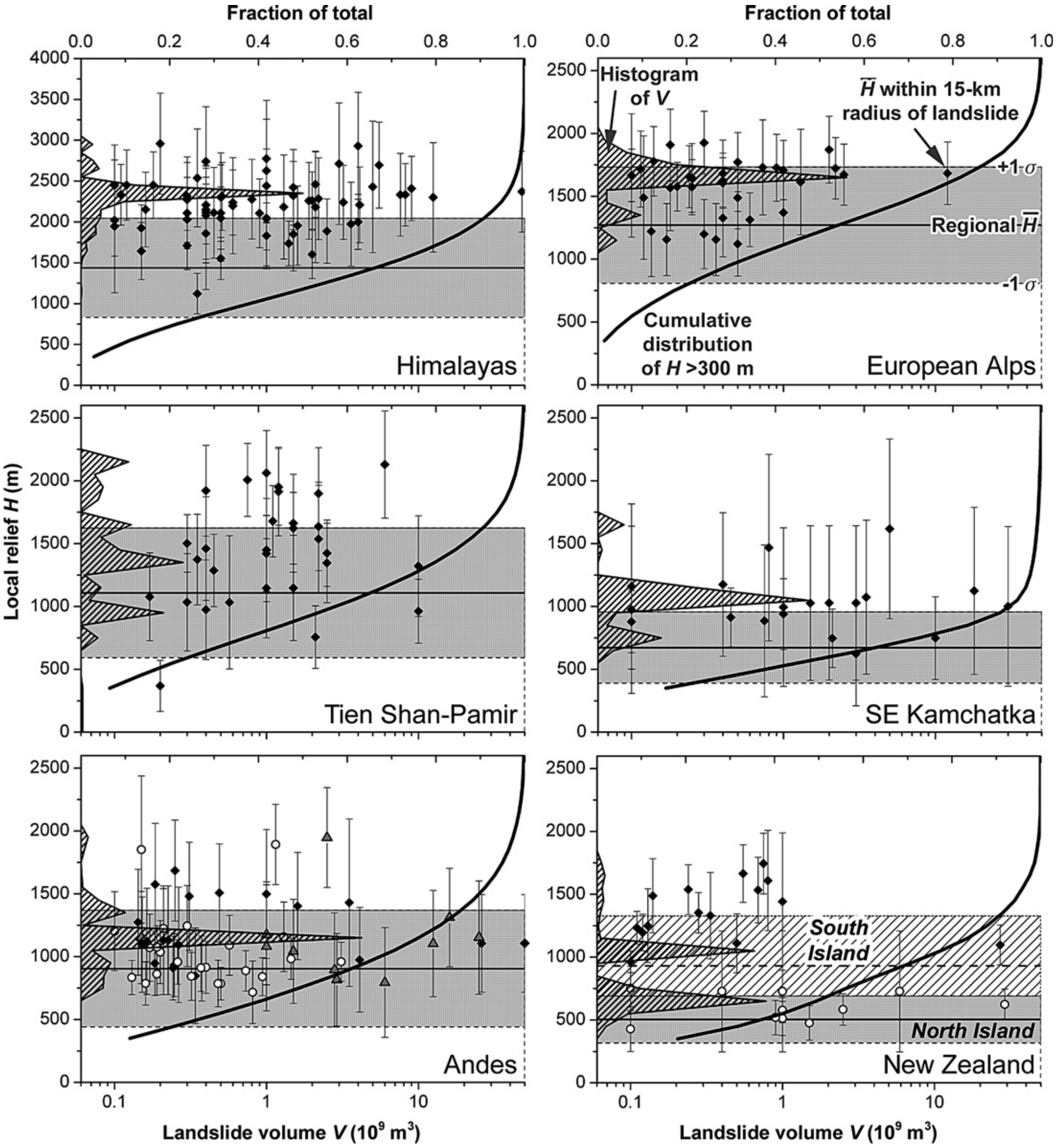

Fig. 3. Relationship between local relief H and volumes of giant landslides in selected mountainous terrain (see caption of Fig. 2 for explanation). Black curves are cumulative percentage distributions of $H>300$ m normalized by area. Grey boxes delimit $\pm 1\sigma$ of H about the orogen-scale mean $\bar{H}$ (horizontal line). Hatched histograms show fraction of total landslide volume. White circles and black diamonds in Andes data are landslides in glaciated and non-glaciated terrain, respectively; grey triangles are volcanic landslides. Additional hatched area for New Zealand data applies to South Island only; white circles and black diamonds are North and South Island landslides, respectively.

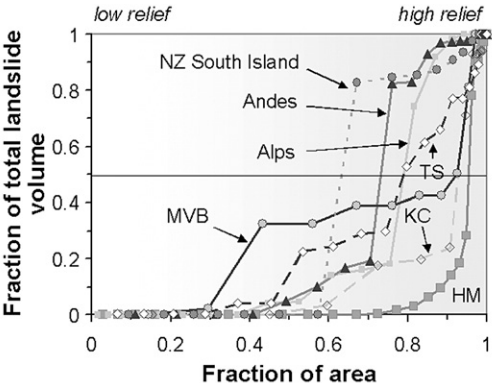

Fig. 4. Distribution of the fraction of total debris volume produced by giant landslides in relation to relief in selected mountain belts and volcanic arcs; HM = Hi-malayas, KC = Kamchatka, MVB = Trans-Mexican Volcanic Belt, TS = Tien Shan-Pamir. Most of the volume is associated with the steepest parts of the landscape.

eastern Himalayan syntaxis (Shang et al., 2000). Other mountain belts in the region, such as the Tien Shan and Pamir, show a less pronounced clustering of giant landslides in the steepest parts of the landscape (Fig. 3). For example, most of the known giant landslides in the Tien Shan have occurred in areas where $\bar{H}$ is within 1σ of the regional average. We observe similar trends in the European Alps and the Andes, where more than half of giant landslides are found in the steepest 18% and 27% of the landscape, respectively. In volcanic arcs, such as southeast Kamchatka, giant landslides are chiefly debris avalanches limited to individual volcanic edifices, which contain most of the regional relief within a very small fraction of the landscape (Fig. 3).

The preferential occurrence of giant landslides in steep terrain becomes even more evident when the distribution of their volumes is considered. In the Himalayas, >70% of the total volume of giant landslides has been produced in the steepest 5% of the landscape (Fig. 4). And, in Kamchatka and the Trans-Mexican Volcanic Belt, more than half of the volume of giant landslides is associated with the steepest 7% of the landscape. Given that $\bar{H}$ correlates well with local slope angles at the length scale of our investigation (Montgomery and Brandon, 2002), we expect a comparable dominance of giant landslides in areas with higher slope angles on average, that is those believed to be closer to threshold conditions and thus subject to higher erosion rates.

3.2. Giant landslides in subcritical relief

Notwithstanding the general trend shown in Fig. 3, giant landslides are not exclusively confined to the steepest parts of mountain belts. Several giant slope failures are located in areas where mean local relief is below the regional average, which we term ”subcritical” relief. In the tectonically active fold-and-thrust belt of North Island, New Zealand, for example, several landslides are associated with soft Tertiary mudstones and sandstones in hilly terrain with a mean local relief $\bar{H} \sim 500 \pm 190$ m (Fig. 3). The causes of giant slope failure in this terrain are thought to be linked to rapid erosional exposure of extensive low-angle, low-strength flexural slip surfaces of tectonic origin (Beetham et al., 2002). Values of apparent basal friction along these bedding-parallel shear planes are below those of residual angles of friction published for soils and most likely require seismic ground acceleration to trigger failure (Beetham et al., 2002). Thus, giant landslides may occur episodically, even if the landscape adjusts mainly to rapid fluvial incision by small-scale landsliding (Reid

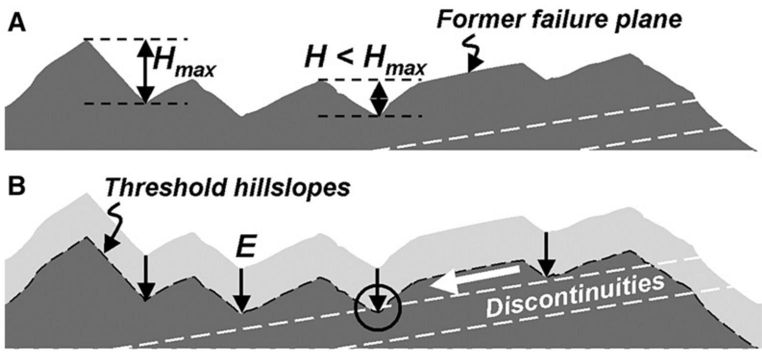

Fig. 5. Cartoons showing low-angle rock-mass discontinuities that precondition softrock terrain to giant landslides. A. Mean local relief $\bar{H}$ is substantially less than that of the regional maximum $\bar{H}_{max}$. B. Constant relief is maintained by rapid fluvial incision E (black arrows) and concomitant landsliding on threshold hillslopes. Exposure of discontinuities on the dip slope (black circle) triggers catastrophic failure on a drainage-basin scale (white arrow). Based on case studies in Beetham et al. (2002).

and Page, 2003; Litchfield and Berryman, 2006 (Fig. 5). In this case, earthquake cycles together with incision rates and the length and spacing of major rock-mass discontinuities determine the magnitude and frequency of giant slope failures.

One of the largest landslides in our dataset occurred in consolidated alluvial sediments in an intracontinental setting of moderate to low relief. The 5×10^{10} m^3 Baga Bogd earth-block slide in the Gobi Altai, Mongolia, travelled on a nearly flat, 15 km-long basal shear plane in lacustrine sediments over a vertical distance of only 300 m (Philip and Ritz, 1999). Aridity precludes rainfall or fluvial undercutting as the trigger. Thrust-induced loading of alluvial sediment wedges on proximal lake deposits along the fault-bounded piedmont may have eventually caused the sediments to collapse (Fig. 14 in Bayasgalan et al. (1999)). In this case, the preparatory mechanism for giant slope failure is tectonically sustained, range-front aggradation, rather than erosion.

In both of the regions mentioned above, giant landslides are conditioned by a combination of soft rocks, extensive low-angle discontinuities, and high rates of fluvial bedrock incision or tectonically driven loading. These factors may outweigh high mean local relief as a prerequisite for large-scale slope failure. Other examples of giant landslides in subcritical relief include the Saidmarreh rock avalanche in the fold-and-thrust topography of the Zagros Mountains, Iran ($V = 2.4 \times 10^{10}$ m^3; $\bar{H} \sim 850$ m), and several failures along mountain range fronts in the western USA, including the Blackhawk rock avalanche ($V = 2.8 \times 10^8$ m^3; $\bar{H} \sim 490$ m).

Many of the largest landslides in the Andes occur in subcritical relief (Hermanns and Strecker, 1999). For example, most giant slope failures in northern Patagonia occur in areas of subcritical relief in formerly glaciated valleys cut into Pliocene plateau basalts (Fig. 3). These young valleys are perpendicular to the folds and thrusts of Andean deformation (Folguera et al., 2004), and have mean local relief on average lower than fault-controlled valleys in other parts of the Andes.

Comparing the heights of individual landslides H_L, here defined as the maximum elevation difference between head scarp and deposit toe, to values of local relief H, in their vicinity supports the observation that giant landslides do not necessarily affect the highest available relief in a given region. On average, sliding masses extended over a vertical range H_L of 1.6 ± 0.9 km (Table 1), indicating the presence of high hillslopes at the failure sites. Two-thirds of the landslides descended > 50% of the maximum local relief, but only half of them descended more than the mean local relief (Fig. 6).

4. Giant landslides and erosion rates

Based on the assumption that mean local relief is a proxy for long-term erosion rates at the regional scale (Montgomery and Brandon, 2002), giant landslides in regions close to the limiting relief are contributors to some of the highest erosion rates documented. Eq. (1) suggests that, on average, these slope failures are associated with values of $E \sim 4.2 \pm 0.2$ mm yr^{-1}. To obtain a regionally more detailed view, we computed first-order

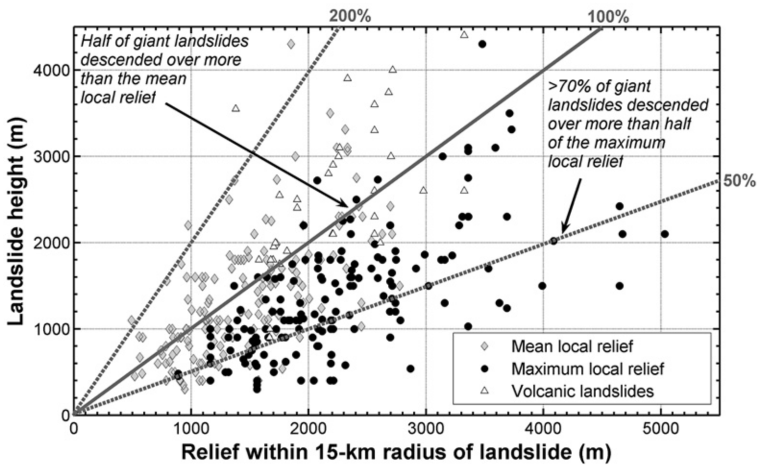

Fig. 6. Relationship between landslide height H_L and mean ($\bar{H}$) and maximum (H_{max}) local relief within a 15-km radius of giant landslides. Diagonal lines are ratios of H_L to $\bar{H}$. The relief affected by volcanic debris avalanches tends to be underestimated by $\bar{H}$. The seven non-volcanic outliers for which $H_L > H_{max}$ are landslides with extreme runout or where pre-failure relief was significantly higher than present relief. See text for explanation.

minimum estimates of erosion caused by giant Late Pleistocene and Holocene landslides in selected mountain belts. We did so by dividing the total volume of individual landslide clusters by the contributing catchment area and the time elapsed between the oldest event and the present. In almost all cases, the elapsed time includes the Holocene, thus ensuring comparability among the inferred erosion rates (Kirchner et al., 2001). Because all of the landslides are catastrophic, the failed material has been significantly displaced and transported. We are not concerned here with the post-failure delivery of landslide material to the fluvial system.

The total volume of all landslides sampled is 10^{12} m^3. Minimum erosion rates attributable to the largest landslides in ten sampled mountain belts are 0.01 mm yr^{-1}, and maximum rates are up to 0.3 mm yr^{-1}. This range reflects differences in topography, tectonics, climate, lithology, and the area over which they were averaged. Specific yields, and thus averaged erosion rates, vary considerably and are highest in small drainage basins. For instance, four historic reactivations of the Tsaoling rock slide/rock avalanche in the Ching-Shui Creek basin, Taiwan, are responsible for an average yield of 5.6×10^6 m^3 km^{-2} yr^{-1} (Chigira et al., 1999). Three giant late Holocene landslides account for nearly 5% of the erosion in the Marsyandi River basin, Central Nepal, assuming an average erosion rate of 7 mm yr^{-1} over the past 10,000 yr (Pratt-Sitaula et al., 2004). This contribution increases to 8% if Eq. (1), which predicts E=4.3 mm yr^{-1}, is used. Similarly, the four largest Late Pleistocene/Holocene rock avalanches in the Alpenrhein basin in the Swiss Alps have contributed 7% of the total postglacial erosion. We estimate comparable contributions for other Himalayan and Alpine water-sheds and for slopes of large volcanoes in areas such as Japan, Indonesia, and the Trans-Mexican Volcanic Belt.

These estimates are, of course, minimum contributions to the overall denudation accomplished by large-scale landslides in a given area, because they are based on only a few large events. Judging from published data on landslides and magnitude–frequency relationships, it is reasonable to assume that these giant failures make up <0.01% of the total number of landslides in each region for the time spans considered. We thus suspect that the largest events in these areas have been significant contributors to erosion rates in the late Quaternary. The volumes of individual landslides, however, are unrelated to mean local relief or erosion rates in all of the areas studied (Fig. 3). For example, some of the highest rates of uplift and fluvial bedrock incision derived from apatite fission track ages and strath terraces are in the upper Indus River basin, Karakoram Himalaya, increasing from <2 to 10 mm yr^{-1} over a horizontal distance of 50 km (Burbank et al., 1996; Burbank, 2002). There, more than 30 giant late Quaternary rockslides and rock avalanches have so far been identified, the largest ten of which have a total volume of up to 1.65×10^{11} m^3 (Hewitt et al., 1998; Hewitt, 2002). Yet their size distribution does not follow the regional gradient of erosion. It is not the areas with the highest erosion rates, but rather those subject to moderate erosion (2–4 mm yr^{-1}) that host the bulk of these giant landslides (Fig. 7A).

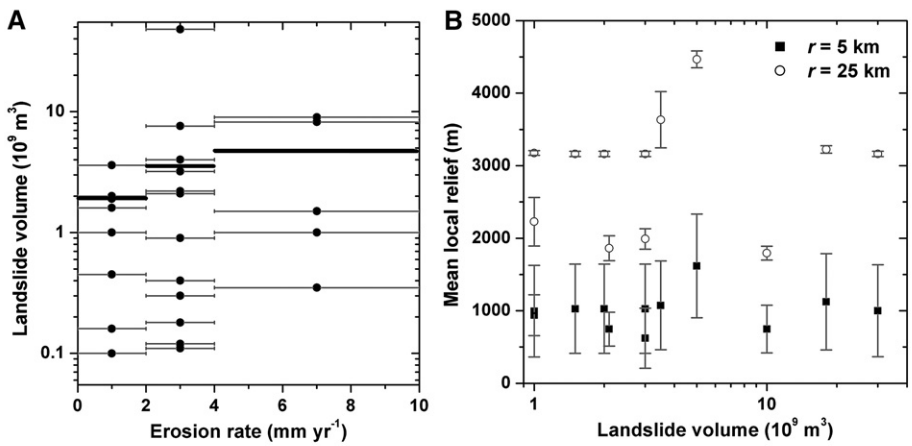

Fig. 7. A. Volumes of selected giant landslides in the upper Indus valley, Karakoram, and their association with long-term erosion rates (0–2, 2–4, >4 mm yr^{-1}) estimated from apatite fission track ages (Burbank, 2002). Most landslides are in zones of moderate erosion; horizontal black lines indicate median volume per category. B. Changes in mean local relief $\bar{H}$ as a function of sampling radius r in southeastern Kamchatka. Although r=25 km (white circles) captures more appropriately the full local relief in this volcanic landscape than does r=5 km, the overall distribution of landslide volume with respect to $\bar{H}$ is not very sensitive to the choice of r.

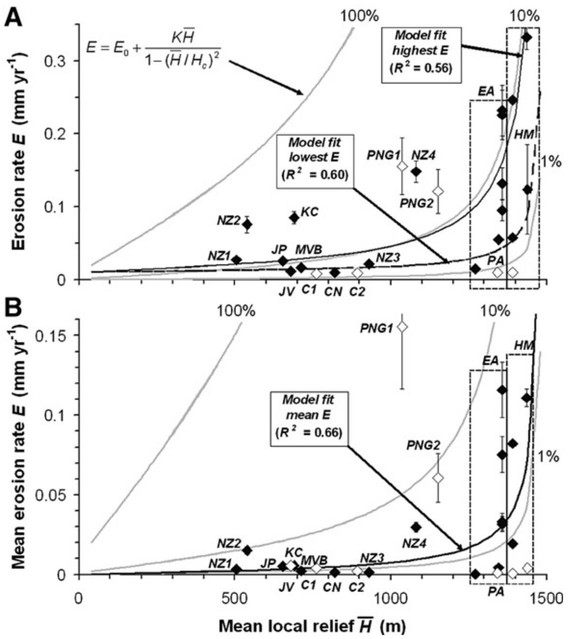

Fig. 8. A. Erosion rates (with vertical error bars) accomplished by Late Pleistocene and Holocene giant landslides increase nonlinearly with orogen-scale mean local relief; CN = south-central China, EA = European Alps, HM = Himalayas, JP = Japan, KC = Kamchatka, MVB = Trans-Mexican Volcanic Belt, New Zealand: NZ1 = North Island, NZ2 = Eastland, NZ3 = South Island, NZ4 = Fiordland, PA = Pamir, Papua New Guinea: PNG1 = Markham River, PNG2 = Finisterre Range. The leftmost grey curve is derived from Eq. (1); grey curves to the right are 10% and 1% fractions. Black solid and hatched curves are model fits for minimum and maximum inferred erosion rates, respectively. Open diamonds indicate range estimates that were not included. B. Same as above, with erosion rates normalized by number of landslides.

The estimated erosion rates of giant landslides in selected mountain belts and volcanic arcs, however, seem to increase with mean local relief (Fig. 8). We fitted Eq. (1) to the data using fixed values of E_0= 0.01 mm yr^{-1} and H_c=1500 m. The resulting explanation of variance is low (R^2=0.28), mainly because of the large number of minimum estimates. We therefore split the dataset and considered the lowest and highest inferred erosion rates separately, for which we obtained values of K=4.4×10^{-6} (±0.9×10^{-6}) yr^{-1}, and 2×10^{-5} (±0.3×10^{-5}) yr^{-1}, respectively (Fig. 8A). In a subsequent step, we kept only E_0 constant. Values of K=6×10^{-5} (±2×10^{-5}) yr^{-1}, and H_c=1692 (±165) m for the seven highest inferred erosion rates explain 77% of the variance. Although we obtained several better fits, we retained this result because H_c is closest to the original value used (Montgomery and Brandon, 2002). Data points with poorly constrained error ranges were omitted from the analysis. Overall, in more than half of the sampled cases, giant landslides contributed >7% to long-term erosion rates predicted by Eq. (1) (Fig. 8A). We note, however, that some of the studied regions have higher actual erosion rates than suggested by this relationship. For example, the Tertiary fold-and-thrust belt of eastern North Island, New Zealand, has mean erosion rates of up to 5 mm yr^{-1} (Litchfield and Berryman, 2006) at a value of $\overline{H}$ that is ~1 km below that of the theoretical value. Also, erosion rates of giant debris avalanches in southeast Kamchatka make up 37% of the regional rate derived from Eq. (1). Using values of E available in the literature, we find that, on average, giant landslides are responsible for 5% of the total erosion in the mountain belts studied.

A similar nonlinear relationship, with K=5.2×10^{-6} (±7.3×10^{-7}) yr^{-1}, is obtained if the erosion rates are normalized by the number of giant landslides in each area. Here, we set E_0=0.0001 mm yr^{-1} because we assume a lower relevance of chemical erosion rates to individual slope failures (Fig. 8B). The hyperbolic trend of per-event rates indicates that in areas of high relief the average contribution of individual giant landslides to total erosion rates may increase. Although the explanations of variance from these model fits are only moderate, the relations nevertheless provide evidence of a significant increase of giant landslide erosion rates with mean local relief.

5. Discussion: Implications and limitations

Most of the largest terrestrial landslides on Earth are clustered in tectonically active mountain belts and volcanic arcs; half of them occur in the steepest part of these landscapes (Fig. 3). There the interaction between tectonic uplift and bedrock incision by glaciers and rivers has produced sufficient relief to predispose slopes to catastrophic failures on this scale. The necessary triggers, such as large earthquakes, high-intensity rainstorms, and glacial and fluvial undercutting of slopes, are also common in these areas. In the following, we use our observations on giant landslides in Earth's mountain belts to further refine these orogen-scale quantitative relationships.

The most pronounced, if not singular, cluster of extremely large rockslides and rock avalanches on Earth, both in terms of spatial density and total volume, occurs in the deeply incised valleys of the upper Indus River basin, Karakoram Himalayas, where locally hillslope height exceeds 4 km. There the Indus River cuts through the rapidly uplifting Nanga Parbat-Haramosh Massif, and local relief is as much as 7.2 km from the channel bed to the highest summit, over a distance of about 21 km. However, the highest part of the detachment zones of the giant landslides we have identified lie below 4000 m a.s.l., and one-third are below 3500 m a.s.l. In other words, they derive from slope segments, spurs, or minor interfluves with much less than the total relief available in the region. This observation supports the notion that most of these rock-slope failures discovered to date descended into ice-free but formerly glaciated river valleys and originated on rock walls oversteepened by glaciers (Hewitt et al., 1998; Hewitt, 2001; Hewitt, 2002). Thus the fraction of the landscape containing upper sections of rock slopes that stood above the glaciers for much or all of their development might indicate the likelihood of giant landslides descending less than the maximum, or even, mean local relief available (Fig. 6). Hence, even in the few small regions of very high mean local relief, the occurrence of giant landslides may be further constrained to a small part of this "stacked" landscape. This constraint does not exclude, however, catastrophic failure of the highest mountain peaks, for example for the $1–1.5 \times 10^{10}$ m^3 Tsergo Ri rockslide, which offset the main divide in the Langtang Himalaya, Nepal (Schramm et al., 1998). We also emphasize that precursory glaciation is not a prerequisite for giant slope failures, as numerous sites are far beyond the limit of Pleistocene glaciation, for example in the Andes of northwest Argentina and the western Tien Shan (Hermanns and Strecker, 1999; Strom and Korup, 2006).

Because landslide height H_L scales moderately with landslide volume V ($R^2 = 0.37$), larger failures should in theory be closer to the limiting relief H_c. This inferred association is consistent with the observation that much of the volume eroded by giant landslides is concentrated in small fractions of mountainous terrain where $\bar{H}$ is highest (Fig. 4). Yet the volume of individual giant landslides does not increase systematically with mean local relief or erosion rate (Figs. 3, 7A). The scatter reflects, to an unknown extent, local differences in seismotectonics, lithology, climate, and geomorphic history. It is also likely that in areas of high erosion former landslide deposits have been eroded to such an extent that they cannot be detected by remote sensing.

Moreover, attainment of substantial mean local relief does not appear to be a prerequisite for giant landslides, as subcritical values ($\bar{H} > 350$ m) are sufficient (Table 1). The topographic control on the occurrence of giant landslides that we emphasize in this paper appears to be less in regions where slopes are developed in soft rocks. There pervasive, low-angle discontinuities in the rock mass, in concert with tectonically driven erosion or loading, promote extremely large landslides whether or not threshold hillslopes have developed (Fig. 5). The largest catastrophic landslides in New Zealand occur in areas of moderate relief on North Island, not in the western Southern Alps where many of the largest slope failures on steeply dipping schistose bedding planes are of a slower and more chronic nature despite overall high denudation rates (Korup, 2006a, b) (Fig. 3). This finding seems counterintuitive, as it is reasonable to assume that in regions of high erosion, such as the upper Indus River basin or the western Southern Alps of New Zealand, giant landslides would develop in particularly strong rocks. Yet we find that giant landslides occur in all major rock types; they are not limited to strong rocks, and frequent small slope failures do not preclude giant ones at the same site. We consider the orientation and spacing of large discontinuities at the hillslope scale to be more important than the strength of the rock itself as a determinant of landslide size. The availability of potential large failure volumes is thus set not solely by lithology, but also by the relationship between slope and failure-plane orientation.

We surmise that numerical models of landscape evolution that solely use critical relief thresholds for landslide triggering may underestimate the role of large catastrophic events. We also infer that, substituting $\bar{H}$ for a stage in orogenic development (Montgomery, 2001), giant landslides may occur throughout most of the lifetime of mountain belts, irrespective of the presence of threshold hillslopes, landscape transience, or topographic steady state.

Any increase in mean local relief, for example due to deglaciation of overdeepened trough valleys, to values approaching the limiting relief necessitates a substantial increase in erosion rate (Montgomery and Brandon, 2002). Because giant landslides are important erosional agents near the limiting relief in the mountain belts we studied, their frequency or size must increase to provide the necessary rate response. Indeed, our data indicate that the inferred *minimum* contribution of giant landslides, as well as their proportional contribution to *overall* erosion rates E (including those by rivers, glaciers, and other mass movements), increases nonlinearly with $\bar{H}$. We stress that these estimates are independent of the number of events or the timescale over which they are averaged. The model proposed by Montgomery and Brandon (2002) fits this trend reasonably well (Eq. (1); curve 'Montgomery and Brandon, 2002' in Fig. 1; Fig. 8). With respect to the values of E predicted by Eq. (1), Fig. 8A suggests that giant landslides may be slightly more important contributors to total erosion in areas of lower mean local relief (curve 'Burbank et al., 1996' in Fig. 1). A similar result is obtained when relaxing the assumption of $H_c = 1500$ m; using fixed values of E_0 and H_c does not reveal trends in the relative contribution of giant landslides to total erosion with changes in mean local relief. However, we note that Eq. (1) produces underestimates of E in some of the regions studied. We caution that high erosion rates may also lead to more rapid removal of geomorphic evidence and therefore potential undersampling of previous events (Fig. 7A). Future work will need to address whether the proportion of large-scale slope failures in overall landslide denudation rates will change with mean local relief. Finally, we stress the stochastic nature of slope failure; the nonlinear increase of landslide erosion rates with mean local relief reflects an increase in the number of potentially unstable sites as terrain becomes steeper. It does not imply, though, that giant landslides are the sole drivers of relief maintenance. Neither does it suggest that $\bar{H}$ is a reliable predictor of the locations of such large slope failures.

Our analysis carries several caveats. First, measuring mean local relief within a moving window is sensitive to changes in the radius of the window, r, and does not completely capture the full relief in volcanic arcs, in particular where the radius of individual edifices exceeds r (Fig. 6). We suspect that we either underestimated $\bar{H}$, and thus E, in some volcanic arcs or that the relationship developed has not been calibrated for the highly localised relief distributions in these areas. Use of a larger window size adequately captures the full vertical extent of the landscape around individual volcanoes, but does not significantly change the overall distribution of landslide volume with mean local relief (Fig. 7B). Another potential limitation of the method is that $\bar{H}$ is, by definition, lower along mountain fringes and basin margins than in the cores of mountain belts, where many giant landslides occur (Fig. 2B). Second, deriving mean local relief, $\bar{H}$, from present-day topography ignores changes in relief because of Quaternary climate oscillations. Contemporary topography in mountains masks repeated valley deepening during glaciation and valley filling during interglaciations. Sediment thickness above glacially scoured bedrock can be >1 km thick, and many hillslopes in alpine terrain attained their maximum relief during terminal Pleistocene deglaciation (Eyles et al., 1990; Persaud and Pfiffner, 2004). Third, our analysis does not account for the relief-modifying effects of giant slope failures (Korup, 2006a, b). Detachment of large-scale rock masses involved catastrophic migration and lowering of ridge crests up to 15 km in length (Strom and Korup, 2006). In most such cases, the initial pre-failure hillslope topography cannot be reconstructed. Valley-filling landslide deposits are up to 1 km thick (Table 1) and have in places quantities of sediment trapped behind them that are one or two orders of magnitude larger (Hewitt, 1999; Bookhagen et al., 2005). These sediment wedges have not only impeded fluvial bedrock incision but also further reduced local relief over reaches tens of kilometres long in postglacial time (Korup, 2006a, b; Korup et al., 2006).

6. Conclusions

About half of a worldwide sample of the largest terrestrial landslides have occurred in small portions of tectonically active mountain belts and volcanic arcs where mean local relief and erosion rates are highest. Most of the volume of these mainly bedrock failures is concentrated there, and the proportional contribution of giant landslides to erosion rates increases nonlinearly with mean local relief. These observations imply that hillslope and relief adjustment in areas of high denudation is partly aided, if not significantly accommodated, by these large events, although they may not always extend over the full range of relief available at a site. However, giant landslides are not restricted to areas of highest mean local relief or largest slope angles. They have also occurred along fault-bounded, mountain-range fronts and in tectonically active areas of moderate relief, where large-scale discontinuities and low rock-mass strength control slope stability, whether or not threshold hillslopes have developed. We suspect that numerical landscape evolution models that use critical relief thresholds for landsliding may underestimate the contribution to erosion by large events.

Acknowledgements

This contribution was funded by EU FP6 STREP Contract No. 081412 ("IRASMOS"). We thank three anonymous referees and C. Jaupart for their helpful comments on an earlier version of this paper.

References

Augustinus, P.C., 1995. Glacial valley cross-profile development: the influence of in situ rock stress and rock mass strength, with examples from the Southern Alps, New Zealand. Geomorphology 14, 87–97.

Bayasgalan, A., Jackson, J., Ritz, J.F., Carretier, S., 1999. Forebergs, flower structures, and the development of large-intra-continental strike–slip faults: the Gurvan Bogd fault system in Mongolia. J. Struct. Geol. 21, 1285–1302.

Beetham, R.D., McSaveney, M.J., Read, S.A.L., 2002. Four extremely large landslides in New Zealand. In: Rybar, J., Stemberk, J., Wagner, P. (Eds.), 1st European Conference on Landslides. Swets & Zeitlinger, Prague, pp. 97–102.

Bookhagen, B., Thiede, R.C., Strecker, M.R., 2005. Late Quaternary intensified monsoon phases control landscape evolution in the northwest Himalaya. Geology 33, 149–152.

Burbank, D.W., 2002. Rates of erosion and their implications for exhumation. Mineral. Mag. 66, 25–52.

Burbank, D.W., Leland, J., Fielding, E., Anderson, R.S., Brozovic, N., Reid, M.R., Duncan, C., 1996. Bedrock incision, rock uplift and threshold hillslopes in the northwestern Himalayas. Nature 379, 505–510.

Capra, L., Macias, J.L., Scott, K.M., Abrams, M., Garduno-Monroy, V.H., 2002. Debris avalanches and debris flows transformed from collapses in the Trans-Mexican Volcanic Belt, Mexico — behavior, and implications for hazard assessment. J. Volcanol. Geotherm. Res. 113, 81–110.

Chigira, M., Wang, W.N., Furuya, T., Kamai, T., 2003. Geological causes and geomorphological precursors of the Tsaoling landslide triggered by the 1999 Chi-Chi earthquake, Taiwan. Eng. Geol. 68, 259–273.

Collot, J.Y., Lewis, K., Lamarche, G., Lallemand, S., 2001. The giant Ruatoria debris avalanche on the northern Hikurangi margin, New Zealand: result of oblique seamount subduction. J. Geophys. Res. Solid Earth 106, 19271–19297.

Densmore, A.L., Ellis, M.A., Anderson, R.S., 1998. Landsliding and the evolution of normal-fault-bounded mountains. J. Geophys. Res. 103(B7), 15203–15219.

Eisbacher, G.H., Clague, J.J., 1984. Destructive mass movements in high mountains: hazard and management. Geol. Surv. Can. Paper 84-16 (230p.).

Eyles, N., Mullins, H.T., Hine, A.C., 1990. Thick and fast: sedimentation in a Pleistocene fiord lake of British Columbia. Geology 18, 1153–1157.

Folguera, A., Ramos, V.A., Hermanns, R.L., Naranjo, J.A., 2004. Neotectonics in the foothills of the southernmost central Andes (37–38S): evidence of strike–slip displacement along the Atinir-Copahue fault zone. Tectonics 23. doi:10.1029/2003TC001533.

Hermanns, R.L., Strecker, M.R., 1999. Structural and lithological controls on large Quaternary rock avalanches (sturzstroms) in arid northwestern Ar gentina. Geol. Soc. Amer. Bull. 111, 934–948.

Hewitt, K., 1999. Quaternary moraines vs catastrophic rock avalanches in the Karakoram Himalaya, northern Pakistan. Quat. Res. 51, 220–237.

Hewitt, K., 2001. Catastrophic rockslides and the geomorphology of the Hunza and Gilgit river valleys, Karakoram Himalaya. Erdkunde 55, 72–93.

Hewitt, K., 2002. Styles of rock avalanche depositional complexes in very rugged terrain, Karakoram Himalaya, Pakistan. In: Evans, S.G., DeGraff, J. (Eds.), Catastrophic Landslides: Effects, Occurrence, and Mechanisms, Reviews in Engineering Geology. Geological Society of America, Boulder, CO, pp. 345–378.

Hewitt, K., 1998. Catastrophic landslides and their effects on the upper Indus streams, Karakoram Himalaya, northern Pakistan. Geomorphology 26, 47–80.

Kirchner, J.W., Finkel, R.C., Riebe, C.S., Granger, D.E., Clayton, J.E., King, J.G., Megahan, W.F., 2001. Mountain erosion over 10 yr, 10 k.y., and 10 m.y. time scales. Geology 29, 591–594.

Korup, O., 2006a. Effects of large deep-seated landslides on hillslope morphology, western Southern Alps, New Zealand. J. Geophys. Res.-Earth Surf. 111, F01018. doi:10.1029/2004JF000242.

Korup, O., 2006b. Rock-slope failure and the river long profile. Geology 34, 45–48.

Korup, O., Strom, A.L., Weidinger, J.T., 2006. Fluvial response to large rock- slope failures — examples from the Himalayas, the Tien Shan, and the Southern Alps in New Zealand. Geomorphology 78, 3–21.

Litchfield, N., Berryman, K., 2006. Relations between postglacial fluvial incision rates and uplift rates in the North Island, New Zealand. J. Geophys. Res.-Earth Surf. 111, F02007. doi:10.1029/2005JF000374.

Malamud, B.D., Turcotte, D.L., Guzzetti, F., Reichenbach, P., 2004. Landslide inventories and their statistical properties. Earth Surf. Processes Landf. 29, 687–711.

Montgomery, D.R., 2001. Slope distributions, thresholds hillslopes, and steady-state topography. Am. J. Sci. 301, 432–452.

Montgomery, D.R., Brandon, M.T., 2002. Topographic controls on erosion rates in tectonically active mountain ranges. Earth Planet. Sci. Lett. 201, 481–489.

Persaud, M., Pfiffner, O.A., 2004. Active deformation in the eastern Swiss Alps: post-glacial faults, seismicity and surface uplift. Tectonophysics 385, 59–84.

Philip, H., Ritz, J.F., 1999. Gigantic paleolandslide associated with active faulting along the Bogd fault, Gobi-Altay, Mongolia. Geology 27, 211–214.

Ponomareva, V.V., Melekestsev, I.V., Dirksen, O.V., 2006. Sector collapses and large landslides on late Pleistocene–Holocene volcanoes in Kamchatka, Russia. J. Volcanol. Geotherm. Res. 158, 117–138.

Pratt-Sitaula, B., Burbank, D.W., Heimsath, A., Ojha, T., 2004. Landscape disequilibrium on 1000–10,000 year scales, Marsyandi River, Nepal, central Himalaya. Geomorphology 58, 223–241.

Reid, L.M., Page, M.J., 2003. Magnitude and frequency of landsliding in a large New Zealand catchment. Geomorphology 49, 71–88.

Schmidt, K.M., Montgomery, D.R., 1995. Limits to relief. Science 270, 617–620.

Schramm, J.M., Weidinger, J.T., Ibetsberger, H.J., 1998. Petrologic and structural controls on geomorphology of prehistoric Tsergo Ri slope failure, Langtang Himal, Nepal. Geomorphology 26, 107–121.

Shaller, P.J., 1991. Analysis and Implications of Large Martian and Terrestrial Landslides, Phd. California Institute of Technology.

Shang, Y.J., Yang, Z.F., Li, L.H., Liu, D., Liao, Q.L., Wang, Y.C., 2003. A super-large landslide in Tibet in 2000: background, occurrence, disaster, and origin. Geomorphology 54, 225–243.

Siebert, L., Glicken, H., Ui, T., 1987. Volcanic hazards from Bezymianny- and Bandai-type eruptions. J. Volcanol. 49, 435–459.

Strom, A.L., Korup, O., 2006. Extremely large rockslides and rock avalanches in the Tien Shan mountains, Kyrgyzstan. Landslides 3, 125–136.

Vanneste, M., Mienert, J., Bunz, S., 2006. The Hinlopen Slide: a giant, submarine slope failure on the northern Svalbard margin, Arctic Ocean. Earth Planet. Sci. Lett. 245, 373–388.

Weidinger, J.T., 2006. Predesign, failure and displacement mechanisms of large rockslides in the Annapurna Himalayas, Nepal. Eng. Geol. 83, 201–216.

Wen, B., Wang, S., Wang, E., Zhang, J., 2004. Characteristics of rapid giant land-slides in China. Landslides 1, 247–261.

Whipple, K.X., Kirby, E., Brocklehurst, S.H., 1999. Geomorphic limits to climate-induced increases in topographic relief. Nature 401, 39–43.